

Chemical Science

Accepted Manuscript



This is an *Accepted Manuscript*, which has been through the Royal Society of Chemistry peer review process and has been accepted for publication.

Accepted Manuscripts are published online shortly after acceptance, before technical editing, formatting and proof reading. Using this free service, authors can make their results available to the community, in citable form, before we publish the edited article. We will replace this *Accepted Manuscript* with the edited and formatted *Advance Article* as soon as it is available.

You can find more information about *Accepted Manuscripts* in the [Information for Authors](#).

Please note that technical editing may introduce minor changes to the text and/or graphics, which may alter content. The journal's standard [Terms & Conditions](#) and the [Ethical guidelines](#) still apply. In no event shall the Royal Society of Chemistry be held responsible for any errors or omissions in this *Accepted Manuscript* or any consequences arising from the use of any information it contains.



www.rsc.org/chemicalscience



Journal Name

ARTICLE

High Symmetry or Low Symmetry, It Is a Question – High Performance Dy(III) Single-ion Magnets by Electrostatic Potential Design

Received 00th January 20xx,
Accepted 00th January 20xx

DOI: 10.1039/x0xx00000x

www.rsc.org/

Wen-Bin Sun,^{a,b} Peng-Fei Yan,^b Shang-Da Jiang,^a Bing-Wu Wang,^{*a} Yi-Quan Zhang,^a Hong-Feng Li,^b Peng Chen,^b Zhe-Ming Wang^a and Song Gao^{*a}

A series of mononuclear lanthanide Zn-Dy-Zn type single-molecule magnets (SMMs) were synthesized and magnetically characterized. The four molecules ($[\text{Zn}_2(\text{L}^1)_2\text{DyCl}_3]\cdot 2\text{H}_2\text{O}$ (**1**), $[\text{Zn}_2(\text{L}^1)_2\text{Dy}(\text{MeOH})\text{Br}_3]\cdot 3\text{H}_2\text{O}$ (**2**), $[\text{Zn}_2(\text{L}^1)_2\text{Dy}(\text{H}_2\text{O})\text{Br}_2]\cdot [\text{ZnBr}_4]_{0.5}$ (**3**) and $[\text{Zn}_2(\text{L}^2)_2\text{DyCl}_3]\cdot 2\text{H}_2\text{O}$ (**4**)) all display remarkable magnetic relaxation behavior with relatively high energy barrier and hysteresis temperature although possessing low local geometry symmetry of center Dy(III) ions. The ab initio studies revealed that the symmetry of charge distribution around Dy(III) ion is the key factor to determine the relaxation of the SMMs. The four complexes orient their magnetic easy axes along the negative charge dense direction concerning the first coordination sphere. The entire molecular magnetic anisotropy was therefore controlled by the single substituent atom in the hard plane consisting of five coordination atoms (perpendicular to the easy axis), the lower charge distribution on which and closer to the hard plane, the more prominent magnetic slow relaxation displaying. It offers an efficient and rational method to improve dynamic magnetic relaxation of these mononuclear lanthanide SMMs that usually possessing the low local geometry symmetry around lanthanide(III) center.

Introduction

Since the first single-molecule magnet (SMM), Mn_{12}Ac , was discovered in the 1990s, many magnetic molecules exhibiting slow relaxation of magnetization were synthesized and magnetically characterized. Large negative zero-field splitting and ground state spin are regarded as two essential factors to obtain an SMM with high relaxation barrier (U_{eff}) and blocking temperature (T_{B}), which play a crucial role in technological applications of SMMs involving the field of quantum computer, spintronics device and high-density information storage.¹⁻⁶ The intrinsic strong spin-orbit coupling and large magnetic anisotropy render the lanthanide ions as the ideal candidate for constructing SMMs with high relaxation barrier compared to transition metal-based SMMs. Even in the single 4f-center system, *i.e.* mononuclear lanthanide SMMs or single-ion magnets (SIMs), the significant slow relaxations of the magnetization with high energy barriers for magnetization reversal have been observed.⁷ The relative simply structure of

lanthanide SIMs is convenient for chemists to improve the understanding on the magneto-structural correlation.⁸⁻¹⁴ Compared to transition metal system, however, the magnetic structure of lanthanide is more complex due to their strong spin-orbit coupling. Recent researches reveal the single-ion magnetic anisotropy of lanthanide ions is extremely sensitive to the subtle change of ligand field (LF) and the local geometrical symmetry. The electrostatic potential distribution around spin center plays an important role.^{15, 16}

With the fast development of lanthanide based SMMs, the record of reversal barrier of mononuclear SMMs is continuously broken, whereas improving the blocking temperature seems much more difficult. The magnetic hysteresis, as an important criterion of SMMs, was only observed at low temperature. It is mostly ascribed to the faster quantum tunneling of magnetization (QTM) through the barriers, which reduces the thermally activated relaxation across the barrier, commonly referred as the Orbach process, and/or the thermal assisted QTM (TA-QTM). Usually a high axial symmetry around spin center favors suppressing QTM and renders the thermally active Orbach relaxation prominently. Some lanthanide-based molecules possessing high order axial symmetry, such as D_{4d} , D_{3h} , D_{2d} , D_{5h} , C_5 and $C_{\infty v}$ have been designed and synthesized to reduce the QTM and develop novel SMMs with improved energy barriers and blocking temperature.^{11, 17-19} However, the high local symmetry is not easy to achieve due to the intrinsic high coordination numbers and variable coordination modes of lanthanide ions,

^a Beijing National Laboratory of Molecular Science State Key Laboratory of Rare Earth Materials Chemistry and Applications, College of Chemistry and Molecular Engineering, Peking University Beijing 100871, P. R. China. E-mail: wangbw@pku.edu.cn and gaosong@pku.edu.cn

^b Key Laboratory of Functional Inorganic Material Chemistry Ministry of Education, Heilongjiang University, Harbin 150080, P. R. China.

† Electronic supplementary information (ESI) available: Additional magnetic data, additional Figs and computational details. CCDC 929546, 974436, 974437 and 974438 for 1-4. For ESI and crystallographic data in CIF or other electronic format see DOI: 10.1039/x0xx00000x

a low symmetry system is usually observed for the lanthanide-containing complexes.

The electron density distribution of lanthanide(III) ions is strongly angular dependent. It has a preferred orientation under the electrostatic potential generated by the ligand donor atoms. In other words, the charge distribution of ligand provides an efficient way to control the magnetic anisotropy. This principle has been illustrated in terms of “oblate” and “prolate” electron density distributions in a recent review.^{20a} It was shown that for the terbium(III) and dysprosium(III)-based SMMs, the strong anisotropy can be achieved by using axial ligand fields, whereas equatorial ligand fields favour erbium(III)-based SMMs. The former inference has been verified by the archetypal family of phthalocyanine (Pc) complexes [Bu₄N][LnPc₂] (Ln = Tb and Dy) and their analogues, and the latter model has been obtained by few Er-based SIMs with equatorial ligand field.^{19b,21a}

Although there are many exciting works on the lanthanide-based mononuclear and multinuclear SMMs, the relaxation barriers have been reached 938 K⁷ and impressive blocking temperature increased to 14 K (*T_B*),²² there are still some open questions like the source of slow magnetic relaxation of 4f-based SMMs, the relaxation mechanism and/or the key factors influencing the magnetic anisotropy. Therefore, it presents a challenge to design and synthesize an ideal system to study and well understand the relaxation behavior of lanthanide SIMs, for example, does the geometrical or electronic symmetry of molecule determine the relaxation behavior? It is a real complicated task to construct certain charge configuration induced by the coordination donor atoms in ligands because of the high coordination number and flexible coordination model of lanthanide complexes.

Recently, several SMMs studies on Zn–Dy and Zn–Dy–Zn^{19a, 23, 24} type complexes constructed by the Schiff based ligands have revealed that the phenoxo-oxygen donor atoms possess relative larger negative charges than aldehyde-oxygen donor atoms or methoxyl oxygen atoms within ligand. An axial high charge distribution along the magnetic easy axis will enhance the energy barriers of Dy(III)-based SMMs but no impressive hysteresis temperature was achieved. Even in a series of linear Zn(II)–Ln(III)–Zn(II) type molecules,^{23c} in which all the higher electron density induced by four phenoxo-oxygen atoms distributed in the opposite position of the Dy(III) ion, but no significant SMM behavior was observed. Given the very recent report of the first trigonal pyramidal erbium SMM^{21b} that revealed strictly prolate f-electron density is not required to stabilize a crystal field that favors SMM behavior, the geometric design principles to minimize electronic repulsions between the electron densities of the lanthanide ions and the ligands should be used carefully. Especially, for the low symmetric system, the tiny deviation of coordination atoms from the easy axis and/or the hard plane (perpendicular to the easy axis) could introduce the transversal anisotropy component and reduce the *U_{eff}* significantly. Fortunately, we verified this key factors in a series of air-stable mononuclear lanthanide based Zn–Dy–Zn type SMMs formed by salen-type ligands H₂L¹ and H₂L² (Scheme 1 and 2), which possesses the

plentiful phenoxyl and methoxyl oxygen donor atoms with higher and lower negative charges distribution, and they were elaborately placed in nearly parallel and perpendicular arrangement to the easy axis, respectively.

In comparison to the high symmetrical geometry structure usually found in high performance lanthanide SIMs, only a C₂ axis exists through Cl and Dy(III) center in the two of these molecules. There are nine coordinated oxygen atoms in the first coordination sphere of Dy(III) ion, in which five oxygen atoms with lower electron density constitute a hard plane with pseudo C₅ axis surrounding the Dy(III) center, and the phenoxyl atoms with the high electron density locate the two sides of this hard plane. This special electron density distribution results in a significant SMMs behaviour with the magnetic hysteresis at the temperature as high as 12 K and a large relaxation barrier over 430 K. It is more important that one of the coordination atoms in this hard plane could be replaced by other substituents while maintaining the other coordination atoms, which allows us to fine-tune the hard plane in the first coordination sphere, and consequently control the magnetic anisotropy of the molecule. Furthermore, another similar ligand with same inner tetradentate coordination O2O2 site was used to probe the influence beyond the first coordination sphere on the slow magnetic relaxation.

Herein we provide an experimental case involving four novel Zn–Dy–Zn SMMs for exploring the impact of the subtle change of the electron density in the first and second coordination sphere on the dynamic magnetic relaxation behavior.

Experimental

All chemicals and solvents were obtained from commercial sources and were used as received, without further purification. The starting Zn(II) complex [Zn(L)] was synthesized according to the procedure reported by Wong et al.²⁵

Synthesis of complexes 1–4

The similar procedure was employed in preparing all complexes; hence, only complex **1** was described in detail. A solution of DyCl₃•6H₂O (12 mg, 0.03mmol) in methanol (10 mL) was added to a suspension solution of ZnL¹ (27 mg, 0.06 mmol) in acetonitrile. The mixture was stirred and heated under reflux (6 hours). After cooled to room temperature, the solution was filtered. The crystals of product were obtained by diffusing diethyl ether slowly into the solution in a sealed container. Elemental analysis calcd (%) for **1**, C₄₄H₄₀Cl₃DyN₄O₁₀Zn₂: C, 44.62; H, 3.40; N, 4.73; found: C, 44.70; H, 3.12; N, 4.73. ZnL² was used instead of ZnL¹ for synthesizing **4**, DyBr₃ was used instead of DyCl₃•6H₂O for synthesizing **2**, ethanol and DyBr₃ were used instead of methanol and DyCl₃•6H₂O when synthesizing **3**. Elemental analysis calcd (%) for **2**, C₄₅H₄₆Br₃DyN₄O₁₂Zn₂: C, 39.51; H, 3.39; N, 4.10; found: C, 39.88; H, 3.43; N, 4.20; Elemental analysis calcd (%) for **3**, C₄₄H₃₈Br₄DyN₄O₉Zn_{2.5}: C, 37.42; H, 2.71; N, 3.97; found: C, 37.60; H, 2.80; N, 4.02. Elemental analysis calcd (%) for **4**,

$C_{44}H_{50}Cl_3DyN_4O_9Zn_2$: C, 44.84; H, 4.28; N, 4.75; found: C, 44.79; H, 4.11; N, 4.65.

Physical measurements

Elemental (C, H and N) analyses (EA) were performed on a Perkin-Elmer 2400 analyzer. Samples were fixed by eicosane to avoid movement during magnetic measurements. The static magnetic measurements and alternating-current (ac) susceptibility measurements under an oscillating field of 3 Oe in the frequency range from 1 to 1000 Hz were performed on the polycrystalline samples using a Quantum-Design MPMS magnetometer, respectively. The magnetization hysteresis loops were measured on a Quantum Design MPMS XL-5 SQUID magnetometer at low sweep rate (100-300 Oe/min). For the sweep rate more than 50 Oe/s, the measurement was performed on the Quantum Design PPMS magnetometer. Magnetic data were corrected for the diamagnetism of the samples using Pascal's constants and the sample holder.

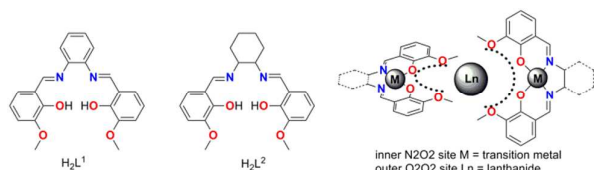
Crystallographic data collection and refinement

Data were collected on a Nonius Kappa CCD diffractometer with Mo $K\alpha$ radiation ($\lambda = 0.71073 \text{ \AA}$). Empirical absorption corrections were applied using the Sortav program. All structures were solved by the direct method and refined by full-matrix least squares on F^2 using the SHELX program.²⁶ H atoms were located in a difference Fourier synthesis.

Results and discussion

Synthesis and characterization

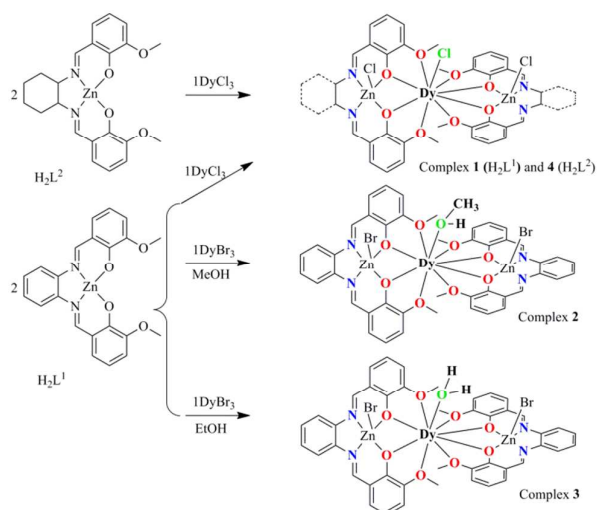
We utilize the classic compartment salen-type Schiff base as the ligand which has been widely used to build d-f heteronuclear complexes with the magnetic or luminescent properties. We also developed a series of salen-type dinuclear and tetranuclear SMMs with the relative rigid and aromatic cyclic backbone ligand.²⁷ In order to construct a more simple system *i. e.* mononuclear lanthanide SMMs, the hexadentate (N2O2O2) salen-type Schiff base N,N' -bis(3-methoxysalicylidene)phenylene-1,2-diamine (H_2L^1) and N,N' -bis(3-methoxysalicylidene)-1,2-diaminocyclohexane (H_2L^2) were used (Scheme 1), in which the inner N2O2 site was occupied initially by diamagnetic Zn(II) ions leaving the outer O2O2 cavity for the larger lanthanide ions, consequently the two Zn-L fragments encapsulated a Zn-Dy-Zn type compounds were obtained.



Scheme 1 The schematized construction of these SMMs.

All the complexes **1-4** were obtained using the similar synthesis procedures. The starting Zn-based precursors $[ZnL]$ ($L = L^1$ and L^2) was synthesized according to the procedure reported by Wong et al.²⁵ Reaction of ZnL complex with $DyCl_3$

or $DyBr_3$ in 2:1 mole ratio gave four complexes with general formula $[Zn_2(L^1)_2DyCl_3] \cdot 2H_2O$ (**1**), $[Zn_2(L^1)_2Dy(MeOH)Br_3] \cdot 3H_2O$ (**2**), $[Zn_2(L^1)_2Dy(H_2O)Br_2] \cdot [ZnBr_4]_{0.5}$ (**3**) and $[Zn_2(L^2)_2DyCl_3] \cdot 2H_2O$ (**4**) (Scheme 2). When complex **1** was obtained, we notice that the Cl^- anion in the nine-coordinated environment surrounding Dy(III) center is prone to be substituted to fine-tune the local coordination geometry and further possibly control the mononuclear magnetic anisotropy of Dy(III) ion.



Scheme 2 The synthesis procedure for **1-4** and their core structures, the green coordination atoms represent the substitutable positions.

As the first strategy the Br^- anion was used to replace Cl^- , however, the bromine is too large to locate at the chlorine position, a methanol molecule unexpectedly occupies the position and resulting in the complex **2**. Then, we try to replace the MeOH molecule by EtOH, interestingly, another unexpected structure, complex **3** was obtained, in which the MeOH molecule in **2** was replaced by a H_2O molecule. The synthesis of **1-3** indicates the spatial position of the replaceable Cl^- in **1** is suitable to accommodate a molecule with the size between Cl^- and MeOH. These complexes provide the opportunity to fine tune the first coordination sphere surrounding Dy(III) center. In order to explore the influence of far coordination region, another salen-type Schiff based N,N' -bis(3-methoxysalicylidene)-1,2-diaminocyclohexane (H_2L^2 , Scheme 1, 2) was used to build $[Zn_2(L^2)_2DyCl_3]$ (**4**) and maintain the first coordination sphere configuration.

The geometric structures of complex **1-4** are depicted in Fig. 1, Fig S1 and the crystal data are listed in Table S1. Complex **1** and **4** are constructed from ligands H_2L^1 and H_2L^2 , they nearly possess the same coordination atoms in the first coordination sphere. They crystallize in the same monoclinic space group $C2/c$. **2** and **3** are constructed by H_2L^1 but crystallized in triclinic, $P-1$ and monoclinic, $P21/c$ space group respectively due to the different recrystallization conditions. In the four complexes, the Zn(II) ions invariably occupy the internal N2O2 site and further completed the five-coordinated square-pyramidal geometry by one Cl^- (for **1** and **4**) or Br^- (for **2** and **3**) at the

apical position. The Dy(III) ion is encapsulated by the two ZnL fragments with outer O2O2 coordination site, lying nearly perpendicularly to each other, consequently located in a pocket consisting of eight oxygen and one substitutable atoms. The Dy(III) ions of complex **1-4** have the similar first coordination sphere, only differ in the outer diamine moiety. As for **1**, **2** and **3**, the first coordination sphere surrounding the Dy(III) center differ in the ninth substituent group Cl⁻, MeOH and H₂O besides the same eight oxygen atoms from two ligands (Fig. 1). The shortest distances of neighboring Dy(III) ions in **1-4** are longer than 10 Å due to the large ZnL spacer.

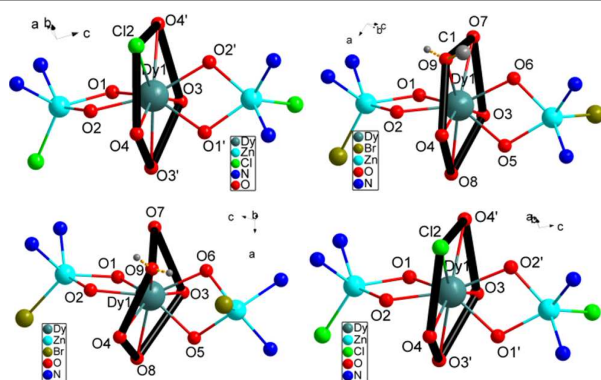


Fig. 1 The core structure for **1** (top left), **2** (top right), **3** (bottom left), **4** (bottom right), the outer backbone of ligands and counter anions are omitted for clarity.

The local symmetry of Dy(III) ions in complex **1-4** was analysed using the parameter *S* of continuous-shape-measures (CShMs) method,^{28,29} which allowed us to quantify the degree of distortion of the coordination sphere (*S* value equals 0, corresponds to the perfect polyhedron and the larger value indicates the more deviated from the ideal geometry). The relative large *S* values of 2.1-3.6 (Table S2) reveal that the coordination environment of Dy(III) center in **1-4** is in a low geometrical symmetry. The structures are almost in the same degree of deviation to the ideal spherical capped square antiprism (*C*_{4v}), spherical tricapped trigonal prism (*D*_{3h}) and Muffin-shape (*C*_s), respectively, in which *C*₄ and *C*₃ axial symmetry are often observed for SIMs. In fact, as for the monoclinic *C*_{2/c} crystal system for **1** and **4**, there is a *C*₂ symmetric axis in the molecules through Cl and Dy atoms (Fig. S2, black dashed line).

Interestingly, the further inspection to the coordination environment of the Dy(III) center in **1-4** reveals that there is a five-member ring consisted of four methoxyl oxygen atoms from two ligands and one chlorine atom (for **1** and **4**) or oxygen atom in MeOH (for **2**) or in H₂O (for **3**) (Fig. 1, thick black ring). It is almost perpendicular to the Zn-Dy-Zn direction. Given a least-square plane defined by the five coordination atoms, the deviations of the individual atoms from this least-square plane are not large except for complex **3** (Table S3). The charge density from ab initio calculations (Table S4) reveals that the lower charge density distributes on the pentagonal ring consisting of four methoxyl oxygen atoms and one substitutable atom (Fig. 1, thick black ring). In contrast, larger negative charge distributes on phenoxy oxygen atoms, which

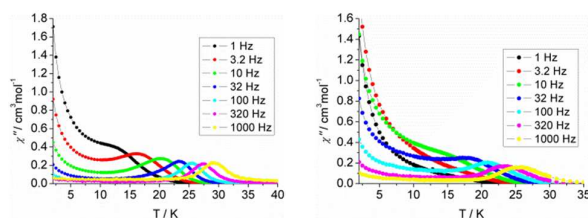
results in the shorter bonding distance of Dy-O and an axially enhanced LF. The axial electron density distribution are found to induce a high energy barrier but the magnetic hysteresis was not detected.²³

Magnetic behavior

The static magnetic measurements were performed on the polycrystalline samples using a Quantum-Design MPMS magnetometer. The temperature dependence of magnetic susceptibility $\chi_M T$ for **1-4** is shown in Fig. S3. The values of $\chi_M T$ are 14.09, 14.27, 14.04 and 14.29 cm³Kmol⁻¹ at 300 K for **1-4** respectively, which are in good agreement with the theoretical value for one free Dy(III) ion (*S* = 5/2, *L* = 5, ⁶*H*_{15/2}, *g* = 4/3). On lowering the temperature, the $\chi_M T$ product decreases gradually, which is likely due to the thermal depopulation of the Ln(III) Stark sublevels. The magnetization of **1-4** from zero to 50 kOe dc field at 2, 3, 5 and 8 K are shown in Fig. S4. The maximum values of magnetization reaching 4.9, 4.8, 4.9 and 5.1 μ_B and the lack of saturation at 50 kOe are likely attributed to crystal-field effect and the existence of low lying excited states.

In order to probe the magnetic dynamic behavior of these complexes, the ac susceptibilities at various frequencies and temperatures in the absence of dc field are measured and depicted in Fig. 2 and Fig. S9, S10.

Both in-phase (χ') and out-of-phase (χ'') susceptibilities show significant frequency dependence peaks at relative high temperature range, which clearly indicates the slow relaxation of magnetization arises from SMM properties. The maximum peaks of the out-of-phase signals were found from 10 K to 30 K for an oscillating field range of 1 Hz to 1000 Hz. The first and clear peaks are observed at 3.2, 32, 320 and 3.2 Hz for **1-4** respectively. The increasing of χ' and χ'' below 10 K is indicative of the quantum tunneling of the magnetization (QTM) at a zero dc field. The frequency magnitude of the first maximum peaks for **1-4** reflects the impact of QTM to the SMMs, the lower one mostly indicates the existence of a slower QTM process where the thermally activated Orbach relaxation process occurs prominently. In order to suppress or minimise the QTM it is necessary to lift the degeneracy of the states to prevent the spins relaxing through tunneling. This can be achieved by applying a dc field. As shown in Fig. S11, S12, the χ' and χ'' tails nearly vanished under 1000 Oe dc field and the peaks can be observed even at the lower frequency of 1 Hz, which indicates the QTM is suppressed efficiently.



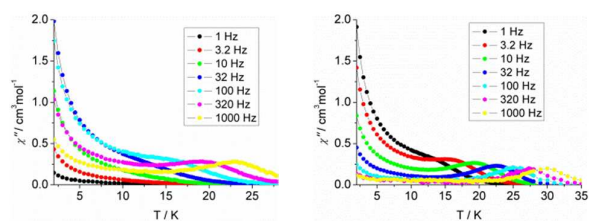


Fig. 2 Temperature dependence of the out-of-phase susceptibility (χ'') plots of **1** (top left), **2** (top right), **3** (bottom left), **4** (bottom right), between 1 and 1000 Hz under zero dc field.

To confirm whether the relaxation in **1-4** is thermally activated mechanism, the natural log of the relaxations, τ extracted from the peak maxima of χ'' , were plotted versus $1/T$ to check for Arrhenius-type linearity which was normally referred to the Orbach relaxation of the magnetization ($\tau = \tau_0 \exp(U_{\text{eff}}/k_B T)$, Fig. 3). It is interesting to note that, the curvature in the $\ln(\tau)$ versus $1/T$ plot under zero field was observed for **1**, and the QTM process was usually responsible for this deviation from Arrhenius-type linearity. Owing to the Kramers nature of Dy(III) ion, at zero field, dipole-dipole and hyperfine interactions should be responsible for the mixing of the two Kramers ground states that allows the zero-field quantum tunneling dynamics of the magnetization. To remove the QTM effect, the ac magnetic susceptibility measurements under applying a 1000 field and on a diluted sample by Y(III) analogue with 1/20 molar ratio were performed. They do efficiently suppress the QTM process with the diminishing χ'' signals at the low temperature range (Fig. S14, S15). It is also noteworthy that the plots of $\ln(\tau)$ versus $1/T$ either under 1000 field or for the diluted sample still exhibit obvious curvature which indicates perhaps another relaxation pathway is also operative (Fig. 3 left). The presence of multiple relaxation processes is possible as reported in a few SIMs.³⁰⁻³² In view of this, we fitted the magnetic data with the equation 1 considering the spin-lattice relaxation of both Raman and Orbach processes.³³

$$1/\tau = CT^n + \tau_0^{-1} \exp(-U_{\text{eff}}/k_B T) \quad (1)$$

The first and second terms correspond to the Raman and Orbach processes, respectively. In general, $n = 9$ for Kramers ions, but when both the acoustic and optical phonons are considered depending on the structure of energy levels, n values between 1 and 6 are reasonable.³⁴ Equation 1 affords $U_{\text{eff}}/k_B = 430$ K, $\tau_0 = 7.4 \times 10^{-11}$ s in the absence of dc field, $U_{\text{eff}}/k_B = 481$ K, $\tau_0 = 1.3 \times 10^{-11}$ s under 1000 Oe dc field, and $U_{\text{eff}}/k_B = 434$ K, $\tau_0 = 7.0 \times 10^{-11}$ s for the samples with 20 times magnetic site dilution, respectively (see Fig. 3 left, Table S6). Complex **4** displays the similar relaxation behavior as **1**, the same equation 1 was used to fit the plot of $\ln \tau$ versus $1/T$ and give the energy barrier of $U_{\text{eff}}/k_B = 398$ K with $\tau_0 = 3.5 \times 10^{-10}$ s.

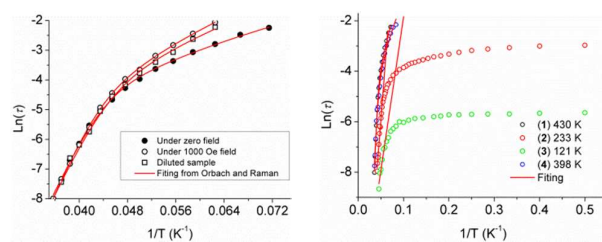


Fig. 3 Plots of $\ln(\tau)$ versus $1/T$ at zero, 1000 Oe dc field and the sample with 20 times magnetic site dilution for **1** (left) and (right) for **1-4** under zero field. The red solid lines represent the fitting of the frequency-dependent data by Equation 1 for **1** and **4** and the pure Arrhenius fitting at the high-temperature linear region for **2** and **3**.

Whereas for **2** and **3**, there is an apparent cross procedure from temperature-dependent regime associated with thermally active Orbach relaxation to a temperature-independent regime related to the QTM upon lowering the temperature. The high-temperature region (19-24 K for **2**, 17-22 K for **3**) was fitted using the pure Arrhenius law, which resulted in the estimated effective energy barrier to the magnetization reversal of $U_{\text{eff}}/k_B = 233$ K with $\tau_0 = 2.5 \times 10^{-8}$ s for **2** and $U_{\text{eff}}/k_B = 121$ K with $\tau_0 = 8.5 \times 10^{-7}$ s for **3** in the absence of dc field. The relaxation time of QTM for **2** and **3** are extracted from ac susceptibility as 51.3 ms and 3.5 ms, respectively, whereas the slower QTM process occurred in **1** and **4**. In our case, the relaxation barriers increase in the order of **3** < **2** < **1**, **4** corresponding to their QTM time trends.

Generally, the effective relaxation barrier of Orbach process is comparable with the energy difference of the ground and first excited states. The CASSCF/CASPT2/RASSI method was used to calculate the fine energy spectrum of complex **1-4** (see computation details in SI). The obtained energy gap 497 K and 398 K between the ground and the first excited states in **1** and **4** are close to the fitting values extracted from the modified Arrhenius analysis, whereas apparent deviation observed in **2** and **3**. The origin of this discrepancy may be related with the presence of additional relaxation processes (for example, tunneling in the ground state induced by dipolar-dipolar interactions or vibronic coupling) that are important for the extracted experimental U_{eff} values but were not considered in the U_{calcd} values^{15, 35}. Moreover, the value of U_{eff} in **2** and **3** should be treated with caution owing to the high temperature peak maximum data are limited in the fitting of U_{eff} from the pure Arrhenius fitting. On the other hand, the tunneling effect usually was quantified by the transverse anisotropy component. The calculated values of g_x 0.0012, g_y 0.0018 for **2** and g_x 0.0023, g_y 0.0036 for **3** are larger than g_x 0.0000, g_y 0.0002 for **1** and g_x 0.0002, g_y 0.0005 for **4** (table S5), which confirms the QTM in **2** and **3** with relative larger transverse anisotropy components are pronouncedly than **1** and **4**.

To confirm the SMM behavior of these complexes, magnetic hysteresis, another important characteristic of magnetic bistability of a magnet, was also measured at different temperature on polycrystalline samples (see Fig. 4) with the sweep rate used in a traditional SQUID magnetometer (100-300 Oe·min⁻¹). The significant hysteresis was still detected

under 8 K, 6 K, 4 K and 8 K for **1-4**, respectively. As for **1**, if the sweep rate of the field was increased to 50 Oe·s⁻¹ and 200 Oe·s⁻¹, the hysteretic behavior could be even detected at 10 K and 12 K, respectively (Fig. S7, S8). To the best of our knowledge, these hysteresis temperatures are among the highest ones reported to date for the Dy(III)-based SIMs.^{19a,16b,36}

For the lanthanide-based SIMs, the butterfly type loops were often observed. The close up of the hysteresis at zero field is attributed to the QTM process. To deduce the QTM effect, the 20 times magnetic site dilution samples with Yttrium for **1** are also measured at low temperature. The loop was still recorded well, which indicates that it is the single-ion feature rather than the long-range ordering. A remanence of 1.2 N β and a coercive field of 300 Oe was found at 1.8 K and the open of the loop at zero field could still be observed until 4 K (Fig. S13).

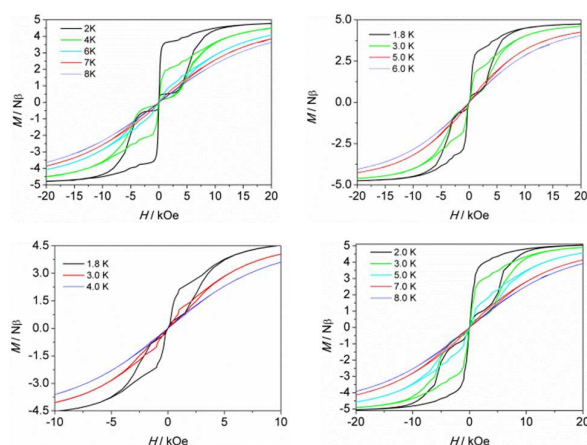


Fig. 4 Magnetization (M) vs. applied dc field (H) on a Quantum Design MPMS XL-5 SQUID magnetometer for **1** (top left), **2** (top right), **3** (bottom left) and **4** (bottom right).

The calculated g values for **1-4** are listed in Table S5. The g_z values close to 20 indicate that the four systems display significant strong uniaxial magnetic anisotropy for Dy(III) ions. However, we noticed that they differ in the energy barriers (U_{eff} , under zero field) and hysteresis temperatures (under the same sweep rate used in a traditional SQUID magnetometer). For **1-4**, the energy barriers and hysteresis temperatures are 430 K, 233 K, 121 K, 398 K and 8 K, 6 K, 4 K and 8 K, respectively. Both of the two parameters increase in the order of **3** < **2** < **1** \approx **4** which is in consist with the g_z values increasing trend 19.7884 (**3**) < 19.8462 (**2**) < 19.9615 (**1**) \approx 19.9658 (**4**). The significant magnetic relaxation behavior mainly arises from the corresponding large magnetic anisotropy. Moreover, the reduced g_z value usually accompanying relative high g_x and g_y values can be considered as the characteristic of transverse anisotropy component. The system with a slower QTM process favours occurrence of the thermally active magnetic relaxations. It is very crucial to make clear that what introduces the transverse anisotropy component, however, the influence factors are very complicated than assume. The symmetry of the local coordination environment is one of the indispensable factors. Usually a relative high axial symmetry

results in a high magnetic anisotropy. The coordination sphere especially within the closest region, even the second peripheral ligand surrounding the magnetic easy axis, will influence the magnetic anisotropy significantly. The direction of the calculated anisotropy axis was shown in Fig. S1 and Table S5, which nearly parallels with the Zn-Dy-Zn direction and being perpendicular (with angle of 90°) to the C_2 axis of the molecule **1** and **4**. The same phenoxy oxygen atoms surround along the principal axis (or J_z vector) with high charge density distribution in **1-4**, which generates a strong easy-axis ligand field (vide infra for ab initio calculations Table S4). On the other hand, the hard plane composed of one substitutable group and four methoxy oxygen atoms possesses the lower charge density distribution (see Fig. S1). The results demonstrate that a joint contribution, combining the enhanced high negative charge distribution along the magnetic easy axis with the decreased electrostatic distribution within the hard plane, may ultimately lead to high performance SMMs capable of retaining their magnetization at more practical temperatures irrespective of the low symmetry of the coordination environment.

In our case, the significant axially high and equatorially low negative charge distribution around the oblate Dy(III) ion induced by ligands are observed which leads to the significant SMMs behaviors. As for the SIMs system, the magnetic anisotropy is related with the fine electronic structures, as described previously, depending on which J_z sublevel of the lanthanide ions has a characteristic electronic distribution. For Dy(III) ions, the pure ground state sublevel with a maximum $|J_z|$ value of 15/2 has a larger electronic distribution on the equatorial plane (hard plane) than along the principal axis, whereas sublevel with a minimum $|J_z|$ value of 1/2 has a larger distribution along the principal axis. If coordination atoms with larger negative charges are located along the axis and/or lower electronic distribution around the equatorial plane, it will strongly stabilizes the former ($m_{15/2}$ state) due to the decreased electron repulsion and leads to significantly easy axial anisotropic ground states, whereas the latter ($m_{1/2}$ state) becomes relatively unstable. Inspecting to the closest electrostatic potential distribution surrounding the Dy(III) center in **1-4**, there is nearly the same charge distribution along the magnetic easy axis, therefore the electron distribution in hard plane was considered as the key factor to introducing transverse anisotropy and QTM, and finally influence the whole molecular magnetic anisotropy.³⁷

However, despite much lower electronic density distributed on the hard plane of **3**, which displayed a relative weak magnetic anisotropy reflected in their slightly smaller calculated g values and SMMs properties with lower energy high and hysteresis temperature. There might be other important factor to determine the single-ion magnetic anisotropy besides the special electrostatic potential distribution pandering to the electron density distributions of the lowest ground states m_j in 4f ions. The more detail inspection to the hard plane reveals that the deviations of five coordination atoms from their least-square plane are different owing to the key substituent coordination atom (Table S3).

Complexes **2** and **3** display relative more apparent deviation from the hard plane than **1** and **4**.

For each 4f-ion, the charge distribution of sublevels with maximum J_z quantum number, characterized by the angle θ_{\max} (the angle from the equatorial plane), will diffuse the maximum electric density.^{20b} For the Tb(III) ion, the maximum distribution angle θ_{\max} found in the equatorial plane is 0° , whereas θ_{\max} increases to 34° for Dy(III) ion.^{23c} Thus the positions of the coordination donor atoms with different deviation from the equatorial plane generate different electronic repulsion strength between the 4f electrons and donor atoms. The relative large repulsion might lead to reduction of anisotropy.^{20a,23c} For our case, the substitutable coordination atom in the equatorial plane of **3** displays the largest deviation (Table S3), followed by **2**, **4**, and **1**. The more deviation from the equatorial plane the more possible meeting in the direction distributing highest electron density between the electrons of Dy(III) and donor atoms, and the electronic repulsion may ultimately lead to a relative weak magnetic anisotropy system, which might be mostly responsible for the different SMMs behavior in **1-4**. On the other hand, the four complexes possess the two axially same coordination phenoxyl atoms along the easy axis, and the five substitutable atom in the hard plane acts as the key adjusting knob, the deviation of which from the hard plane will lead to the distortion of the assumptive pentagonal–bipyramid geometry and consequently influence the molecular magnetic anisotropy.

Conclusions

In summary, a series of air-stable Zn-Dy-Zn lanthanide SIMs displaying remarkable slow magnetic relaxation behavior were facily synthesized. They afford the relative high relaxation energy barrier for the reversal of the magnetization and hysteresis temperature among the Dy(III)-based mononuclear SMMs. More importantly, although they display the significant low geometrical symmetry, only C_2 axis among them, which is much lower than previously reported higher axial symmetry system, the relatively strong magnetic anisotropy and significant SMMs behavior were observed. The magnetic data analysis and theoretical calculations showed that the symmetry of charge distribution around the Dy(III) ion is the key factor to determine the slow relaxation of these molecules. It provides a practical idea to design new lanthanide SMMs despite the lanthanide-containing complexes usually have a high coordination number and flexible coordination geometry.

Acknowledgements

This work was supported by the NSFC (21290171, 21321001, 21102039, 21571008 and 21572048) and the National Basic Research Program of China (2013CB933401, 2010CB934601) and BNLMS (20140108) and Educational Commission of Heilongjiang Province (1254G045, 12541639).

Notes and references

- R. Sessoli, D. Gatteschi, A. Caneschi, M. A. Novak, *Nature*, 1993, **365**, 141.
- D. Gatteschi, R. Sessoli, J. Villain, *Molecular Nanomagnets*, Oxford University Press, Oxford, 2006.
- J. van Slageren, *Top. Curr. Chem.*, 2012, **321**, 199.
- D. Gatteschi, R. Sessoli, *Angew. Chem. Int. Ed.*, 2003, **42**, 268.
- L. Bogani, W. Wernsdorfer, *Nat. Mater.*, 2008, **7**, 179.
- R. Vincent, S. Klyatskaya, M. Ruben, W. Wernsdorfer, F. Balestro, *Nature*, 2012, **488**, 357.
- C. R. Ganivet, B. Ballesteros, G. de la Torre, J. M. Clemente-Juan, E. Coronado, T. Torres, *Chem. Eur. J.*, 2013, **19**, 1457.
- N. Ishikawa, M. Sugita, T. Ishikawa, S.-Y. Koshihara, Y. Kaizu, *J. Am. Chem. Soc.*, 2003, **125**, 8694.
- M. A. AlDamen, J. Clemente Juan, E. Coronado, C. Martí-Gastaldo, A. Gaita-Ariño, *J. Am. Chem. Soc.*, 2008, **130**, 8874.
- (a) S. D. Jiang, B. W. Wang, G. Su, Z. M. Wang, S. Gao, *Angew. Chem. Int. Ed.*, 2010, **49**, 7448; (b) S. D. Jiang, B. W. Wang, H. L. Sun, Z. M. Wang, S. Gao, *J. Am. Chem. Soc.*, 2011, **133**, 4730.
- S. Cardona-Serra, J. M. Clemente-Juan, E. Coronado, A. Gaita-Ariño, A. Camón, M. Evangelisti, F. Luis, M. J. Martínez-Pérez, J. Sesé, *J. Am. Chem. Soc.*, 2012, **134**, 14982.
- D. E. Freedman, W. H. Harman, T. D. Harris, G. J. Long, C. J. Chang, J. R. Long, *J. Am. Chem. Soc.*, 2010, **132**, 1224.
- J. D. Rinehart, J. R. Long, *J. Am. Chem. Soc.*, 2009, **131**, 12558.
- J. J. Le Roy, L. Ungur, I. Korobkov, L. F. Chibotaru, M. Murugesu, *J. Am. Chem. Soc.*, 2014, **136**, 8003.
- D. Aravena, E. Ruiz, *Inorg. Chem.*, 2013, **52**, 13770.
- (a) N. F. Chilton, D. E. Collison, J. L. McInnes, R. E. P. Winpenny, A. Soncini, *Nat. Commun.*, 2013, **4**, 2551; (b) L. Ungur, J. J. Le Roy, I. Korobkov, M. Murugesu, L. F. Chibotaru, *Angew. Chem. Int. Ed.*, 2014, **53**, 4413.
- (a) D. N. Woodruff, R. E. P. Winpenny, R. A. Layfield, *Chem. Rev.*, 2013, **113**, 5110; (b) P. Zhang, L. Zhang, J. K. Tang, *Dalton Trans.*, 2015, **44**, 3923; (c) L. Ungur, S. Y. Lin, J. K. Tang, L. F. Chibotaru, *Chem. Soc. Rev.*, 2014, **43**, 6894; (d) J. K. Tang, P. Zhang, *Lanthanide Single Molecule Magnets*, Springer Berlin Heidelberg press, 2015; (e) S. Gao, *Molecular Nanomagnets and Related Phenomena, Structure and Bonding*, Springer Berlin Heidelberg press, 2015, **164**.
- R. J. Blagg, L. Ungur, F. Tuna, J. Speak, P. Comar, D. Collison, W. Wernsdorfer, E. J. L. McInnes, L. F. Chibotaru, R. E. P. Winpenny, *Nat. Chem.*, 2013, **5**, 673;
- (a) J. L. Liu, Y. C. Chen, Y. Z. Zheng, W. Q. Lin, L. Ungur, W. Wernsdorfer, L. F. Chibotaru, M. L. Tong, *Chem. Sci.*, 2013, **4**, 3310; (b) K. R. Meihaus, J. R. Long, *J. Am. Chem. Soc.*, 2013, **135**, 17952.
- (a) J. D. Rinehart, J. R. Long, *Chem. Sci.*, 2011, **2**, 2078; (b) J. Sievers, *Z. Phys. B: Condens. Matter Quanta*, 1982, **45**, 289.
- (a) P. Zhang, L. Zhang, C. Wang, S. Xue, S. Y. Lin, J. K. Tang, *J. Am. Chem. Soc.*, 2014, **136**, 4484; (b) A. J. Brown, D. Pinkowicz, M. R. Saber, K. R. Dunbar, *Angew. Chem. Int. Ed.*, 2015, **54**, 5864.
- J. D. Rinehart, M. Fang, W. J. Evans, J. R. Long, *J. Am. Chem. Soc.*, 2011, **133**, 14236.
- (a) T. Kajiwara, M. Nakano, K. Takahashi, S. Takaishi, M. Yamashita, *Chem. Eur. J.*, 2011, **17**, 196; (b) A. Watanabe, A. Yamashita, M. Nakano, T. Yamamura, T. Kajiwara, *Chem. Eur. J.*, 2011, **17**, 7428; (c) M. Maeda, S. Hino, K. Yamashita, Y. Kataoka, M. Nakano, T. Yamamura, T. Kajiwara, *Dalton Trans.*, 2012, **41**, 13640; (d) S. Hino, M. Maeda, K. Yamashita, Y. Kataoka, M. Nakano, T. Yamamura, H. Nojiri, M. Kofu, O. Yamamuro, T. Kajiwara, *Dalton Trans.*, 2013, **42**, 2683; (e) M. A. Palacios, S. Titos-Padilla, J. Ruiz, J. M. Herrera, S. J. Pope, E. K. Brechin, E. Colacio, *Inorg. Chem.*, 2014, **53**, 1465.

- (f) A. Upadhyay, S. K. Singh, C. Das, R. Mondol, S. K. Langley, K. S. Murray, G. Rajaraman, M. Shanmugam, *Chem. Commun.*, 2014, **50**, 8838; (g) I. Oyarzabal, J. Ruiz, J. M. Seco, M. Evangelisti, A. Camón, E. Ruiz, D. Aravena, E. Colacio, *Chem. Eur. J.*, 2014, **20**, 14262; (h) I. Oyarzabal, J. Ruiz, E. Ruiz, D. Aravena, J. M. Seco, E. Colacio, *Chem. Commun.*, 2015, **51**, 12353; (i) J. P. Costes, S. T. Padilla, I. Oyarzabal, T. Gupta, C. Duhayon, G. Rajaraman, E. Colacio, *Chem. Eur. J.*, 2015, DOI: 10.1002/chem.201501500.
- 24 H. L. C. Feltham, S. Brooker, *Coord. Chem. Rev.*, 2014, **276**, 1.
- 25 W. K. Lo, W. K. Wong, W. Y. Wong, J. P. Guo, K. T. Yeung, Y. K. Cheng, X. P. Yang, R. A. Jones, *Inorg. Chem.*, 2006, **45**, 9315.
- 26 (a) G. M. Sheldrick, SHELXS-97, Program for X-ray Crystal Structure Solution, University of Göttingen, Germany, 1997. (b) G. M. Sheldrick, SHELXL-97, Program for X-ray Crystal Structure Refinement, University of Göttingen, Germany, 1997.
- 27 (a) P. H. Lin, W. B. Sun, M. F. Yu, G. M. Li, P. F. Yan, M. Murugesu, *Chem. Commun.*, 2011, **47**, 10993; (b) P. F. Yan, P. H. Lin, F. Habib, T. Aharen, M. Murugesu, Z. P. Deng, G. M. Li, W. B. Sun, *Inorg. Chem.*, 2011, **50**, 7059; (c) W. B. Sun, B. L. Han, P. H. Lin, H. F. Li, P. Chen, Y. M. Tian, M. Murugesu, P. F. Yan, *Dalton Trans.*, 2013, **42**, 13397.
- 28 S. Alvarez, P. Alemany, D. Casanova, J. Cirera, M. Llunell, D. Avnir, *Coord. Chem. Rev.*, 2005, **249**, 1693.
- 29 M. Llunell, D. Casanova, J. Cirera, P. Alemany, S. Alvarez, Shape v. 2.0; Universitat de Barcelona: Barcelona, 2010.
- 30 S. Titos-Padilla, J. Ruiz, J. M. Herrera, E. K. Brechin, W. Wernsdorfer, F. Lloret, E. Colacio, *Inorg. Chem.*, 2013, **52**, 9620.
- 31 J. L. Liu, K. Yuan, J. D. Leng, L. Ungur, W. Wernsdorfer, F. S. Guo, L. F. Chibotaru, M. L. Tong, *Inorg. Chem.*, 2012, **51**, 8538.
- 32 E. Colacio, J. Ruiz, E. Ruiz, E. Cremades, J. Krzystek, S. Carretta, J. Cano, T. Guidi, W. Wernsdorfer, E. K. Brechin, *Angew. Chem. Int. Ed.*, 2013, **52**, 9130.
- 33 A. Abragam, B. Bleaney, *Electron Paramagnetic Resonance of Transition Ions*; Clarendon Press: Oxford, U.K., 1970.
- 34 K. N. Shirivastava, *Phys. Status Solidi B*, 1983, **117**, 437.
- 35 (a) J. M. Zadrozny, M. Atanasov, A. M. Bryan, C. Y. Lin, B. D. Rekken, P. P. Power, F. Neese, J. R. Long, *Chem. Sci.*, 2013, **4**, 125; (b) M. Atanasov, J. M. Zadrozny, J. R. Long, F. Neese, *Chem. Sci.*, 2013, **4**, 139.
- 36 R. A. Layfield, *Organometallics*, 2014, **33**, 1084.
- 37 (a) F. Habib, G. Brunet, V. Vieru, I. Korobkov, L. F. Chibotaru, M. Murugesu, *J. Am. Chem. Soc.*, 2013, **135**, 13242; (b) S. K. Singh, T. Gupta, M. Shanmugam, G. Rajaraman, *Chem. Commun.*, 2014, **50**, 15513.